JOURNAL OF CATALYSIS 93, 83–91 (1985)

Surface Properties of $LaNiO_3$: Kinetic Studies of Reduction and of Oxygen Adsorption

J. L. G. FIERRO, J. M. D. TASCÓN, AND L. GONZÁLEZ TEJUCA[1]

Instituto de Catálisis y Petroleoquímica, CSIC, Serrano 119, Madrid 6, Spain

Received April 18, 1984; revised November 13, 1984

The kinetics of reduction and the kinetics of oxygen adsorption on $LaNiO_3$ were studied in a wide range of temperatures. Temperature-programmed reduction showed two reduction steps: (a) of 1 e^- per molecule between 425 and 675 K and (b) of 3 e^- per molecule between 675 and 900 K. In reduction step (a) a distorted $LaNiO_3$ (because of the presence of anion vacancies) was identified by X-ray diffraction; after sintering in He at 1073 K the perovskite structure was destroyed and La_2NiO_4 and NiO were formed. In reduction step (b) La_2O_3 and Ni were formed, these species being better crystallized after sintering at 1173 K. Steps (a) and (b), in the nonsintered samples, were reversible, i.e., after oxidation at 973 K the perovskite structure was newly formed. Reduction in step (a) takes place according to the contracting sphere model while reduction in step (b) is controlled by formation and growth of reduction nuclei. Experimental data in step (b) fit Avrami–Erofeev's equation. Activation energies for reduction steps (a) and (b) were 108 and 221 kJ mol^{-1}, respectively. The kinetics of oxygen adsorption obeyed Elovich's equation, t_0 being calculated by extrapolation to $Z(t) = 0$ of t vs $Z(t)$ plots. The activation energy of adsorption was 38 kJ mol^{-1}. Within the $LaMeO_3$ series, the more easily reducible oxides ($LaNiO_3$, $LaCoO_3$, $LaMnO_3$) were found to be better adsorbents of oxygen and better catalysts for oxidation than the less reducible one ($LaCrO_3$).

INTRODUCTION

Perovskite-type oxides were shown to be catalysts for a number of reactions (*1*), their most important potential application being for oxidation processes (*2*). Bell *et al.*'s results (*3*) provide a basis for assuming that oxides with the perovskite structure could be promising catalytic materials for the synthesis of oxygenated organic compounds (from CO and H_2) with distinctive characteristics from those of supported metal catalysts. $LaNiO_3$ was recently used for the electrocatalytic reduction of O_2 (*4*). Also, La_2NiO_4 derived from the reduction of this perovskite was found to be catalyst for CO oxidation (*5*).

Previous work carried out in this laboratory was directed toward the study of reduction and oxygen adsorption on some perovskite oxides of the series $LaMeO_3$, *Me* being a first-row transition metal (*6*). This work together with those of other authors (*7, 8*) suggested that these parameters play an important role in the catalytic activity of simple and mixed oxides for oxidation reactions.

The catalytic activity profile of $LaMeO_3$ oxides (*Me:* V, Cr, Mn, Fe, Co, or Ni) for CO oxidation exhibited two maxima for $LaMnO_3$ and $LaCoO_3$ (*9*). This behavior should be due to the metal ion in position B of the perovskite structure as ions in position A are generally inactive; in these catalysts the La^{3+} ion is, also, a poor adsorbent of oxygen. $LaNiO_3$ showed a catalytic activity very near to that observed for $LaCoO_3$. From this it could be inferred that the surface properties of these oxides should be, also, similar. In this work the kinetics of reduction with H_2 and also the kinetics of oxygen adsorption on $LaNiO_3$ were studied.

EXPERIMENTAL

Materials. $LaNiO_3$ was prepared by de-

[1] To whom all correspondence should be addressed.

0021-9517/85 $3.00

composition of citrate amorphous precursors as described in detail previously (*10*). Briefly, citrates were precipitated from an equimolecular solution of metal nitrates and citric acid (Merck reagent grade). Their decomposition took place in the conditions previously determined (*10*) (at 1023 K for 4 h in air) for obtaining a single perovskite phase (the BET specific surface area, taking 0.162 nm^2 as cross-sectional area of N_2 molecule, was 4.69 $m^2\ g^{-1}$). The X-ray diffraction pattern of the sample so obtained is given in Fig. 2a.

H_2 (99.995% pure), He (99.995% pure), and O_2 (99.98% pure) were from Sociedad Española del Oxígeno. For storage, H_2 and He were passed through a trap at liquid-N_2 temperature. O_2 was condensed and distilled taking only the middle fraction.

Equipment and methods. The experiments were carried out in a high-vacuum apparatus to which a Cahn 2100 RG microbalance (sensitivity 10^{-6} g) was connected. Thus in the entire system a dynamic vacuum of 10^{-6} mm Hg (1 mm Hg = 133.3 N m^{-2}) could be maintained. For temperature-programmed reduction (TPR) the sample was pumped for 1 h at room temperature (r.t.) and then put in contact with 300 mm Hg H_2; after this the temperature was linearly increased at 4 K min^{-1} with a Stanton Redcroft Eurotherm programmer. The observed weight loss was taken as a measure of the reduction degree in terms of electrons (e^-) per molecule (for 1 e^- per molecule Ni^{3+} is reduced to Ni^{2+}, the weight loss of the sample being 3.26%). For kinetic runs of reduction the sample was pumped at r.t. for 1 h, heated at 4 K min^{-1} up to the desired temperature, and then contacted with 300 mm Hg H_2. The weight loss as a function of time (t) was recorded for about 80 min. For each isothermal run, a fresh sample was used.

For isothermal kinetic runs of O_2 adsorption the sample was outgassed at 773 K for 15 h and then put in contact with 25 mm Hg O_2. After this the adsorption of O_2 (q) as a function of time was recorded. Between two successive experiments the sample was outgassed at 773 K for 15 h. Thermomolecular effects were corrected by means of blank experiments using in the sample side nonporous glass balls and observing reading changes after introducing into the microbalance enclosure 25 mm Hg O_2 at different temperatures.

The X-ray diffractograms were obtained with a Philips PW/1010 diffractometer using Cu$K\alpha$ radiation and a Ni filter. Reductions were carried out in 300 mm Hg H_2 for 2 h and sinterizations in 500 mm Hg He for 2 h at the indicated temperatures. Care was taken of cooling down the samples from reduction or sinterization temperature to r.t. in H_2 or He.

RESULTS AND DISCUSSION

Temperature-Programmed Reduction

TPR results in terms of e^- per molecule versus temperature are given in Fig. 1. As can be observed the reduction of $LaNiO_3$ takes place in two well-defined steps. The first one (a) of 1 e^- per molecule occurs between 425 and 675 K and the second one (b) of 3 e^- per molecule occurs between this last temperature and 900 K. The fact that in step (b) full reduction (3 e^- per molecule) was not reached points to the presence of anion vacancies and therefore to a nonstoichiometric starting sample of formula La

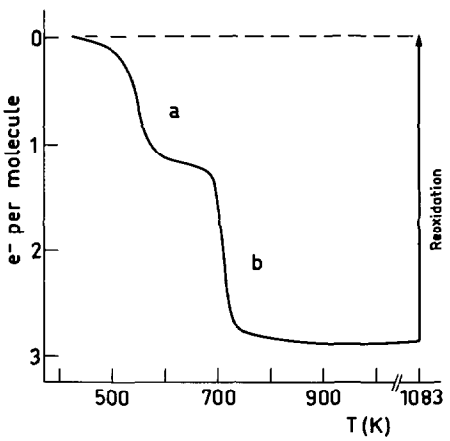

FIG. 1. Temperature-programmed reduction of La NiO_3 in 300 mm Hg H_2 (heating rate, 4 K min^{-1}).

$NiO_{3-\alpha}$. After pumping out the hydrogen and reoxidation with 300 mm Hg of purified air at 1083 K for 1 h the sample regained its initial weight.

Temperatures for reduction levels of 1 and 3 e^- per molecule found in this work are between those reported by Wachowski *et al.* (*11*) and Crespin *et al.* (*12*). These differences must be due to the different rates of heating used. In addition Crespin *et al.* (*12*) found a stable intermediate reduction level of 2 e^- per molecule.

X-Ray Diffraction

To identify the reduced species formed in steps (a) and (b) (Fig. 1) X-ray diffraction patterns (Figs. 2a–e) of the following samples were obtained: After reduction of La NiO_3 at 531 K (2b); after reduction at 513 K, pumping the H_2 (for 1 h at the reduction temperature), and sintering in He at 1073 K (2c); after reduction at 705 K (2d); after reduction at 690 K, pumping the H_2, and sintering at 1173 K (2e) (in cases a–d a fresh sample was used to minimize possible problems of reoxidation derived from handling in air). In Fig. 2a, the pattern of an as-prepared $LaNiO_3$ sample is also given. As can be seen, pattern 2b is similar to that of the initial perovskite (Fig. 2a, cf. the more intense peaks (012) and (110)) although peaks in Fig. 2b are less intense and broader than those of the starting sample. This indicates that a reduction at 531 K does not destroy the perovskite structure; this is preserved although somewhat distorted by the appearance of anion vacancies. Sintering in He (Fig. 2c) causes a profound reorganization of the lattice with destruction of the structure and formation of La_2NiO_4 (*13*), NiO, and also metallic Ni in low concentrations. Similarly, Sis and Wirtz (*14*) and Lombardo *et al.* (*15*) found metallic Co for a bulk reduction of 1 e^- per molecule in $LaCoO_3$. Reduction in step (a) where a mean oxidation state of Ni^{2+} is present can be formulated according to the reaction

$$2\ LaNiO_3 + H_2 \rightarrow La_2NiO_4 + NiO + H_2O. \quad (1)$$

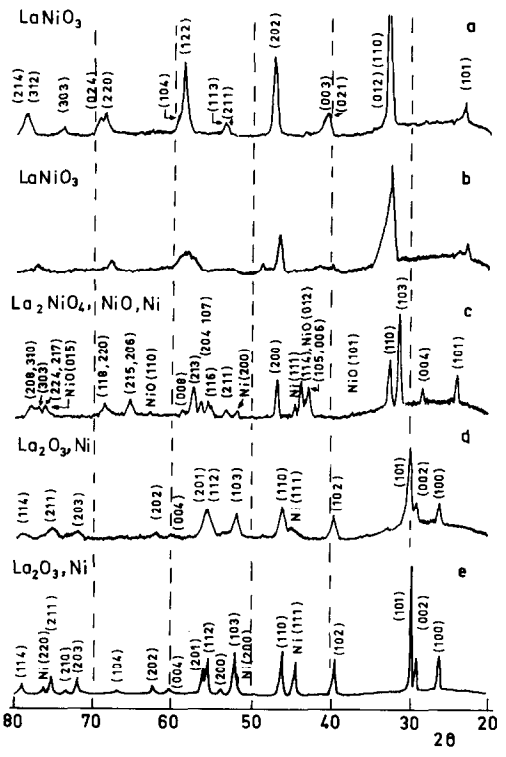

FIG. 2. X-Ray diffraction patterns (Cu$K\alpha$ radiation) of (a) as-prepared $LaNiO_3$; (b) after reduction (300 mm Hg H_2) at 531 K; (c) after reduction at 513 K and sintering (He) at 1073 K; (d) after reduction at 705 K; (e) after reduction at 690 K and sintering at 1173 K.

Crespin *et al.* (*12*) proposed formation of a monoclinic phase of $La_2Ni_2O_5$ for the reduction level of 1 e^- per molecule.

Reduction in step (b) yields La_2O_3 and metallic Ni (Fig. 2d). Peaks are better resolved in Fig. 2e indicating a higher crystallinity of these species after sinterization. Thus, reduction occurs as

$$La_2NiO_4 + NiO + 2\ H_2 \rightarrow La_2O_3 + 2\ Ni + 2\ H_2O. \quad (2)$$

The overall reduction process can be formulated by the reaction

$$2\ LaNiO_3 + 3\ H_2 \rightarrow La_2O_3 + 2\ Ni + 3\ H_2O. \quad (3)$$

To check for reversibility of reduction steps (a) and (b) in Fig. 1, the samples which yielded patterns, b, c, d, and e (Fig.

2) were oxidized at 973 K in air for 1 h. The diffraction patterns obtained after those treatments are given in Fig. 3 (lettering corresponds to this in Fig. 2). Nonsintered samples (Figs. 2b and d) after oxidation yielded a similar pattern to that of the starting $LaNiO_3$ (Figs. 3b and d). Crespin *et al.* (*12*) observed, also, reversibility in the reduction of $LaNiO_3$ to 1 e^- per molecule. Figure 3c contained lines of La_2NiO_4 and NiO, metallic Ni in Fig. 2c being oxidized to Ni^{2+}. After reduction at 690 K, sintering in He and oxidation (Fig. 3e), $LaNiO_3$ as well as simple oxides NiO and La_2O_3 are present. These results indicate that reduction in steps (a) and (b) (Fig. 1) are reversible for the nonsintered samples. In the sintered sample with a larger degree of reduction (step (b), Fig. 1), the reduction is partially reversible. In this process Ni (Fig. 2e) is oxidized to NiO and then the simple oxides react at 973 K to produce $LaNiO_3$ (Fig. 3e). The reversibility would be complete by increasing the oxidation temperature. The sample reduced at 513 K and then sintered, however (Fig. 2c), does not yield

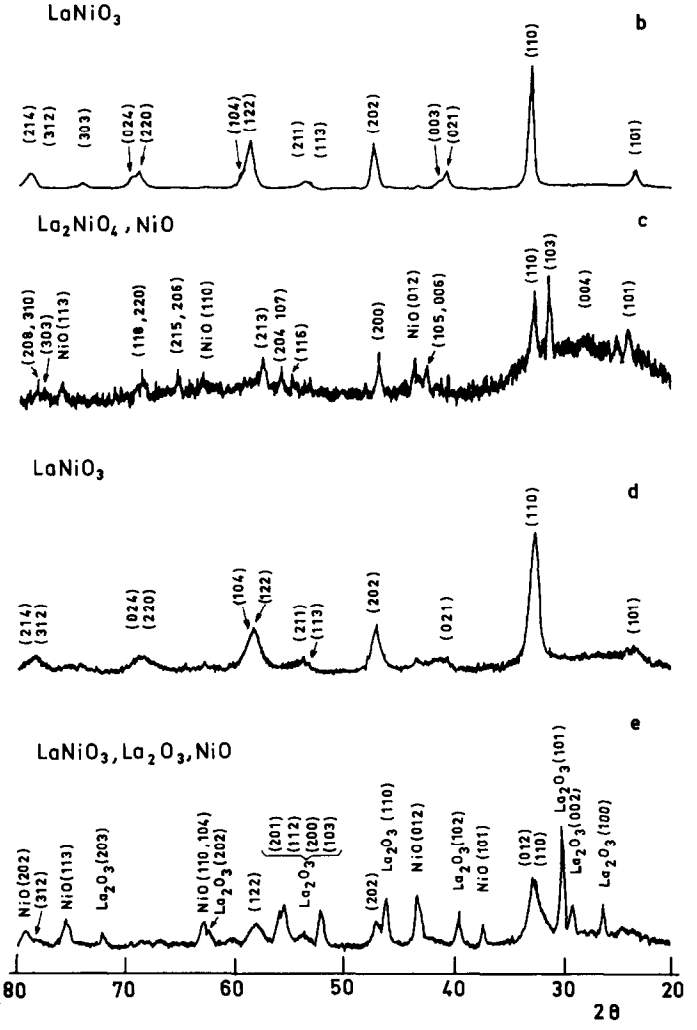

FIG. 3. X-Ray diffraction patterns (Cu$K\alpha$ radiation) of $LaNiO_3$ samples after reduction and oxidation. Patterns (b, c, d, e) correspond to samples (b, c, d, e) in Fig. 2 after oxidation (700 mm Hg in air) at 973 K.

$LaNiO_3$ because of the high stability of the structure of La_2NiO_4. These results are similar to those found by Crespin and Hall (*8*) for $LaCoO_3$ (reversible reduction of 1 and 3 e^- per molecule in the nonsintered samples, and irreversible reduction of 3 e^- per molecule in the sintered sample).

By means of X-ray line broadening measurements and using the Debye–Scherrer equation (*16*), $d = K\lambda/\beta \cos\theta$ (K, constant which was taken as 0.9; λ, wavelength of the X-rays used; β, broadening of the spectral line chosen, calculated by the equation $\beta = \sqrt{B^2 - b^2}$, B being the measured linewidth and b the width measured under the same conditions with a substance composed of particles larger than 1000 Å (1 Å = 10^{-1} nm); θ, diffraction angle of the line considered), particle sizes (d) of the nonsintered and sintered samples of Ni and La_2O_3 were determined. For these calculations the most intense peaks ((111) for Ni and (101) for La_2O_3) in Figs. 2d and e were taken. The results obtained are given in Table 1. By reduction of $LaNiO_3$ at 705 K metallic Ni of a particle size of 60 Å supported on a La_2O_3 matrix is obtained; by sintering in He at 1173 K, d increased by more than an order of magnitude. La_2O_3 with an initial particle size larger than that of Ni (151 Å) underwent, also, an important sinterization. These drastic increases of particle size in the sintered samples hinder the oxidation

TABLE 1

Particle Sizes Determined by X-Ray Line Broadening

Treatment	Peak	B (degrees)	β (radians)	d (Å)
Reduced at 705 K	La_2O_3(101)	0.57	0.0095	151
Reduced at 705 K and sintered	La_2O_3(101)	0.21	0.0021	684
Reduced at 705 K	Ni(111)	1.45	0.0251	60
Reduced at 705 K and sintered	Ni(111)	0.21	0.0021	713

Note. (Cu$K\alpha$) = 1.540 Å.

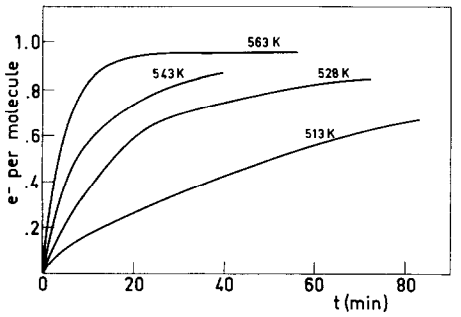

FIG. 4. Kinetics of reduction in 300 mm Hg H_2 at lower temperatures.

of Ni and also the reaction between La_2O_3 and NiO. This accounts for the fully reversible reduction of sample d in Fig. 2 (a single perovskite phase is obtained by oxidation, Fig. 3d) while the reduction in sample e (Fig. 2) is only partially reversible as shown in Fig. 3e.

Kinetics of Reduction

The kinetics of $LaNiO_3$ reduction in H_2 was studied at temperatures (510–570 and 670–730 K) within the zones where the reduction processes (a) and (b) occur (Fig. 1). The kinetic curves plotted in Figs. 4 and 5 point to reduction levels of 1 and 2.68 e^- per molecule, respectively. Kinetic runs in step (b) (Fig. 5) started with a very fast (unmeasurable) reduction (step (a)) after which a slow reduction took place. The fast process was estimated to amount to 1 e^- per molecule and this was considered as the starting point of reduction. The increase in

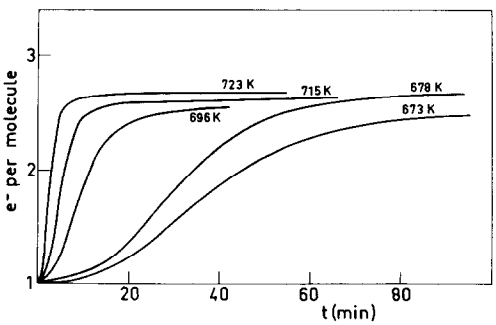

FIG. 5. Kinetics of reduction in 300 mm Hg H_2 at higher temperatures.

the initial reduction rate with temperature shows that the reduction processes (a) and (b) are activated.

While in the first step (a) the reduction rate continuously decreased with t (Fig. 4) in the second step (b) sigmoidal curves were found (Fig. 5). This suggests that the reduction takes place through two different mechanisms. Reduction in step (a) can be interpreted by means of the contracting sphere model assuming that this process starts with a very fast nucleation which results in a total coverage of the $LaNiO_3$ grains by a thin layer of the reduced phase (*17*). This causes a continuous decrease in the rate of the interfacial reaction as the grains of the starting oxide are consumed in the reaction. Reduction in step (b) is controlled by formation and slow growth of reduction nuclei (metallic Ni) on the surface of the reduced phases in step (a) (La_2NiO_4 and NiO). Initially, the reduction rate increases because of the growth of nuclei already formed and the appearance of new ones. The inflection point (Fig. 5) indicates when the reduction nuclei start overlapping. From this point on, the interface of the oxidized and reduced phases and the reduction rate both start decreasing. Sigmoidal reduction curves were observed in unsupported NiO, V_2O_5, and Co_3O_4 while MnO_2 and supported NiO exhibited curves

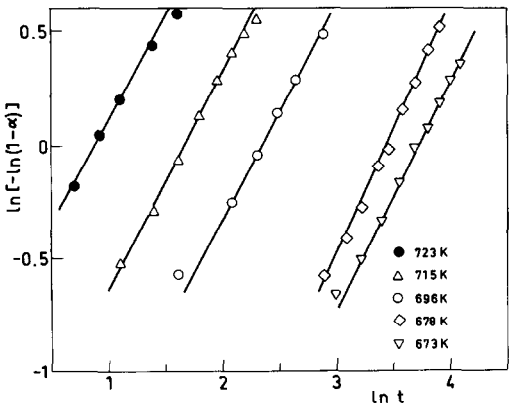

FIG. 6. Linear plots of Avrami–Erofeev's equation for kinetic data in the second reduction step (b).

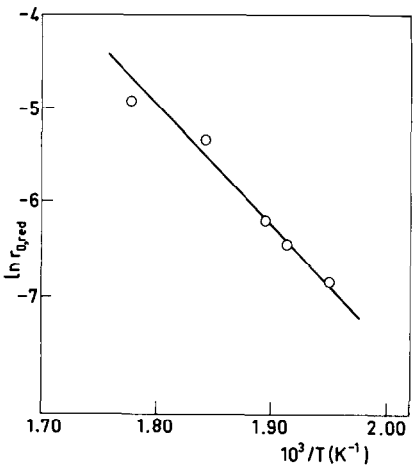

FIG. 7. Arrhenius plot of ln $r_{0,red}$ ($r_{0,red}$, reduction rate at time zero) versus $1/T$. $r_{0,red}$ was derived from reduction kinetic data at 513–563 K.

characteristic of the contracting sphere model (*17, 18*).

The distinction between the two mechanisms of reduction described is somewhat arbitrary because the contracting sphere model starts with a very fast nucleation and the nucleation mechanism ends according to a contracting sphere model (note that reduction in the last branch—after the inflection point—of curves in step (b) is similar to reduction in step (a)).

The kinetic data given in Fig. 5 (step (b)) were analyzed according to Avrami–Erofeev's equation for isothermal transformations (*19*),

$$1 - \alpha = \exp(-kt^n), \qquad (4)$$

(α, reduction degree; n, k, temperature-dependent constants). Linear plots, ln $[-\ln(1 - \alpha)]$ vs ln t are given in Fig. 6; as can be observed, the experimental results fit Eq. (4). The constancy of n (reduction order, calculated from the slope of the straight lines) with T suggests that the mechanism of nuclei growth in this reduction step is not affected by temperature.

The activation energy of reduction (E_{red}) in step (a) was calculated from ln $r_{0,red}$ vs $1/T$ plots ($r_{0,red}$, initial reduction rate determined analytically by fitting the kinetic data

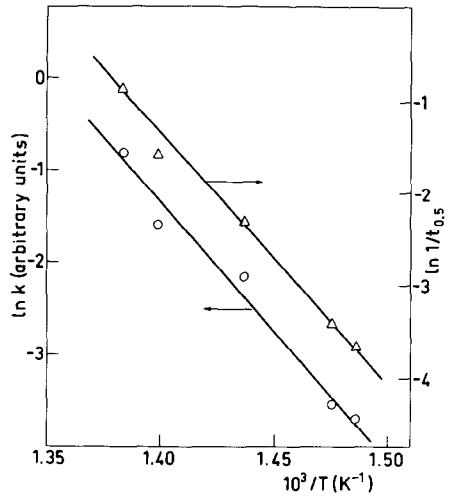

FIG. 8. Arrhenius plots of ln k (k, reduction rate constant) or ln $1/t_{0.5}$ ($t_{0.5}$, time needed for a reduction of 1.84 e^- per molecule, see text) versus $1/T$. k and $t_{0.5}$ were derived from reduction kinetic data at 673–723 K.

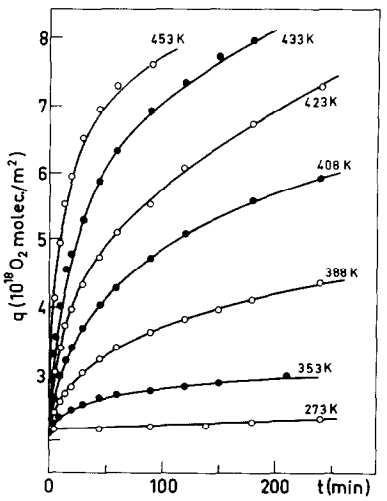

FIG. 9. Integral kinetic data for oxygen adsorption.

to a polynomic function and differentiation to time zero) (Fig. 7). E_{red}, in step (b) was calculated from ln k vs $1/T$ plots (k, constant of Avrami–Erofeev's equation) (Fig. 8); because of the sigmoidal form of the curves, it was also calculated from a plot of ln $t_{0.5}$ vs $1/T$ (*19*) ($t_{0.5}$, time needed to attain a reduction of 1.84 e^- per molecule which is the mean value between the initial, 1 e^- per molecule, and the final, 2.68 e^- per molecule, reduction degrees in Fig. 5). The mean values of E_{red} (Table 2) were 108 and 221 kJ mol^{-1} for 1 and 3 e^- per molecule, respectively, the agreement between methods being 5% or better. These values are lower than the activation energy for reduction of 1 e^- per molecule in $LaMnO_3$ (247 kJ mol^{-1}) showing that this latter oxide is more difficult to reduce than $LaNiO_3$.

Kinetics of Oxygen Adsorption

Integral kinetic data obtained in the zone of activated adsorption are given in Fig. 9. They fit Elovich's equation using t_0 values as calculated by extrapolation of t vs $Z(t)$ plots to $Z(t) = 0$ ($Z(t)$ is the reciprocal of the adsorption rate) (*20*). Coverages of oxygen at $t = 100$ min are given in Table 3 (a cross-sectional area for O_2 molecule of 0.141 nm^2 was taken). They range from 0.3 to about 1 monolayer.

The activation energy of adsorption (E_{ads}) was calculated from ln $r_{o,ads}$ vs $1/T$ ($r_{o,ads}$, initial adsorption rate, calculated from integral kinetic data in a similar way as that described for $r_{0,red}$) and from ln $1/b$ vs $1/T$

TABLE 2

Activation Energies of Reduction

Temperature zone (K)	E_{red} (kJ mol^{-1})	
513–563		108[a]
673–723	227[b]	216[c]

[a] From initial reduction rates.
[b] From Avrami–Erofeev's equation.
[c] From ln $t_{0.5}$ vs $1/T$ (see text).

TABLE 3

Coverages (θ)[a] of Oxygen after 100 min Adsorption

	T (K)						
	273	353	388	408	423	433	453
θ	0.31	0.39	0.52	0.68	0.81	0.99	1.09

[a] A cross-sectional area for the O_2 molecule of 0.141 nm^2 was taken.

TABLE 4

Trends for Oxygen adsorption, Reducibility, and Activity for Total Oxidation on La*Me*O_3 Oxides

O_2 adsorption[a]	$LaCoO_3 \simeq LaMnO_3$	$>$	$LaNiO_3$	$\gg$	$LaCrO_3 > LaFeO_3$
Reducibility	$LaNiO_3 > LaCoO_3 > LaMnO_3$		—	$\gg$	$LaCrO_3$
CO oxidation	$LaCoO_3 > LaNiO_3 > LaMnO_3$	$\gg$	$LaFeO_3$	$>$	$LaCrO_3$
HC oxidation[b]	$LaCoO_3 > LaNiO_3 \simeq LaMnO_3$	$\gg$	$LaCrO_3$	$>$	$LaFeO_3$

[a] At room temperature.
[b] HC: isobutene and propene.

plots (*b*, constant of Elovich's equation). The values of E_{ads} obtained were 38 and 24 kJ mol^{-1}, respectively. As previously observed in the system $O_2/LaCrO_3$ (*6*), the effect of coverage on the activation energy in the latter case is clear as *b* values were calculated from *q* vs ln $(t + t_o)$ plots where $0 < t < 300$ min.

Final Remarks

Within the series of oxides La*Me*O_3, $LaMnO_3$, $LaCoO_3$, and $LaNiO_3$ were the best adsorbents (at room temperature) of oxygen (*21*) and exhibited the highest catalytic activities for CO, isobutene, and propene oxidation (*9, 21*). These reactions were suggested to occur through a mechanism of suprafacial catalysis (*7, 22*) where the catalyst provides orbitals of suitable energy and symmetry for bond formation with reactants and intermediate products. In this mechanism, which occurs without the lattice oxygen participating in the reaction, the adsorbed oxygen must play an important role.

$LaNiO_3$, as reported also for $LaCoO_3$ (*8*), was reduced first to 1 e^- and then to 3 e^- per molecule, these reduction steps being reached at somewhat higher temperatures for the latter oxide. $LaMnO_3$ was reduced to 1 e^- per molecule at 1073 K (*6*). These oxides were found to be better adsorbents of oxygen (*21*) than the oxides more difficult to reduce ($LaCrO_3$ was reduced to only 1.3×10^{-2} e^- per molecule at 1270 K (*6*); $LaFeO_3$ reduced directly to 3 e^- per molecule at 1250 K (*23*), no intermediate reduction step to 1 e^- per molecule being observed; therefore, it would be difficult to compare the reduction behavior of this oxide with those of other members of the La *Me*O_3 series). This is due probably to the fact that the former oxides undergo a certain degree of reduction in the initial outgassing treatment at 773 K with formation of anion vacancies. These vacancies detected in some La*Me*O_3 perovskites (by formation of bidentate carbonates after adsorption of CO_2 on pair sites, O^{2-} ion–anion vacancy) (*24*), should be in lower concentration on the less reducible oxides.

The trends observed for oxygen adsorption, reducibility, and total oxidation of CO, isobutene, and propene on the series of La*Me*O_3 oxides, referred to above, are summarized in Table 4. Although there is not an entirely parallel correspondence among these magnitudes, it is clear that the best catalysts for oxidation reactions ($LaCoO_3$, $LaNiO_3$, $LaMnO_3$) are the best adsorbents (at room temperature) of oxygen and also the oxides which are easier to reduce. On the contrary, $LaCrO_3$ was found to be a poor oxidation catalyst, a poor oxygen adsorbent, and also the member of the La*Me*O_3 series most difficult to reduce.

ACKNOWLEDGMENTS

The authors are indebted to Comisión Asesora para la Investigación Científica y Técnica for sponsorship of this work.

REFERENCES

1. Voorhoeve, R. J. H., "Advanced Materials in Catalysis" (J. J. Burton and R. L. Garten, Eds.), Chap. 5. Materials Science Series, Academic Press, New York, 1977; Happel, J., Hnatow, M.,

and Bajars, L., "Base Metal Oxide Catalysts," Chap. 4. Dekker, New York, 1977.
2. Voorhoeve, R. J. H., Johnson, Jr., D. W., Remeika, J. P., and Gallagher, P. K., *Science* **195,** 827 (1977).
3. Bell, A. T., private communication.
4. Matsumoto, Y., Yoneyama, H., and Tamura, H., *Bull. Chem. Soc. Jpn.* **51,** 1927 (1978).
5. Gunasekaran, N., Meenakshisundaram, A., and Srinivasan, V., *Indian J. Chem. Sect. A* **21,** 346 (1982).
6. Fierro, J. L. G., and González Tejuca, L., *J. Catal.* **87,** 126 (1984); Fierro, J. L. G., Tascón, J. M. D., and González Tejuca, L., *J. Catal.* **89,** 209 (1984).
7. Iwamoto, M., Yoda, Y., Yamazoe, N., and Seiyama, T., *J. Phys. Chem.* **82,** 2564 (1978).
8. Crespin, M., and Hall, W. K., *J. Catal.* **69,** 359 (1981).
9. Tascón, J. M. D., and González Tejuca, L., *React. Kinet. Catal. Lett.* **15,** 185 (1980).
10. Tascón, J. M. D., Mendioroz, S., and González Tejuca, L., *Z. Phys. Chem. Neue Folge* **124,** 109 (1981).
11. Wachowski, L., Zieliński, S., and Burewicz, A., *Acta Chim. Acad. Sci. Hung.* **106,** 217 (1981).
12. Crespin, M., Gatineau, L., Fripiat, J., Nijs, H., Marcos, J., and Lombardo, E., *Nouv. J. Chim.* **7,** 477 (1983).
13. Rabenau, A., and Eckerlin, P., *Acta Crystallogr.* **11,** 304 (1958).
14. Sis, L. B., and Wirtz, G. P., *J. Appl. Phys.* **44,** 5553 (1973).
15. Lombardo, E. A., Tanaka, K., and Toyoshima, I., *J. Catal.* **80,** 340 (1983).
16. Jelinek, Z. K., "Particle Size Analysis," Chap. 2, Series in Analytical Chemistry. Ellis Horwood, New York, 1974.
17. Hurst, N. W., Gentry, S. J., and Jones, A., *Catal. Rev. Sci. Eng.* **24,** 233 (1982).
18. Roman, A., and Delmon, B., *Compt. Rend. C* **273,** 1310 (1971).
19. Keattch, C. J., and Dollimore, D., "An Introduction to Thermogravimetry," 2nd ed., Chap. 5. Heyden, London, 1975.
20. Aharoni, C., and Ungarish, M., *J. Chem. Soc., Faraday Trans. 1* **72,** 400 (1976); **73,** 456, 1943 (1977).
21. Kremenić, G., Nieto, J. M. L., Tascón, J. M. D., and González Tejuca, L., *J. Chem. Soc., Faraday Trans. 1,* in press.
22. Voorhoeve, R. J. H., Remeika, J. P., and Trimble, L. E., *Ann. N. Y. Acad. Sci.* **272,** 3 (1976).
23. Tascón, J. M. D., Fierro, J. L. G., and González Tejuca, L., unpublished results.
24. González Tejuca, L., Rochester, C. H., Fierro, J. L. G., and Tascón, J. M. D., *J. Chem. Soc., Faraday Trans. 1* **80,** 1089 (1984).